



# Biomimetic graphene oxide-cationic multi-shaped gold nanoparticle-hemin hybrid nanozyme: Tuning enhanced catalytic activity for the rapid colorimetric apta-biosensing of amphetamine-type stimulants

Oluwasesan Adegoke<sup>a,\*</sup>, Svetlana Zolotovskaya<sup>b</sup>, Amin Abdolvand<sup>b</sup>, Niamh Nic Daeid<sup>a</sup>

<sup>a</sup> *Leverhulme Research Centre for Forensic Science, University of Dundee, Dundee, DD1 4GH, UK*

<sup>b</sup> *Materials Science & Engineering Research Cluster, School of Science & Engineering, University of Dundee, UK*

## ARTICLE INFO

### Keywords:

Aptamer  
Gold nanoparticle  
Graphene oxide  
Hemin  
Peroxidase mimic

## ABSTRACT

Amphetamine-type stimulants are a class of illicit drug that constitutes a worldwide problem to which intelligence agencies, first responders and law enforcement are tasked with identifying them in unknown samples. We report on the development of a graphene oxide (GO)-cationic multi-shaped gold nanoparticle (AuNP)-hemin hybrid nanozyme as a new biomimetic catalytic-induced aptamer-based colorimetric biosensor platform for amphetamine (AMP) and methamphetamine (MAMP). GO was electrostatically bonded to cationic multi-shaped cetyltrimethylammonium bromide (CTAB)-AuNPs to form a GO-CTAB-AuNP hybrid nanozyme exhibiting enhanced catalytic activity in the presence of hemin. The binding of an MNS 4.1 anticocaine DNA aptamer on the GO-CTAB-AuNP-hemin nanozyme assembly and the subsequent catalytic oxidation by 3,3,5,5-tetramethylbenzidine in the presence of H<sub>2</sub>O<sub>2</sub> ensured that the colorimetric reaction was tuned to selectively detect AMP and MAMP with high sensitivity. Under optimum experimental conditions, AMP and MAMP were quantitatively detected within 1 min with a detection limit of 34.1 ng/mL and 28.6 ng/mL respectively. Selected substances and drugs, known to react positively to Marquis and Mandelin reagents (used in AMP and MAMP presumptive testing) and well-known adulterants, were tested for their affinity to react with the aptamer-based GO-CTAB-AuNP-hemin peroxidase mimic biosensor. The deep blue colorimetric reaction, specific to AMP and MAMP detection, was used as the basis to affirm the selectivity of the aptamer-based GO-CTAB-AuNP-hemin peroxidase mimic biosensor. We believe the colorimetric biosensor developed in this work demonstrates a promising new direction in presumptive testing for AMP and MAMP.

## 1. Introduction

The outcome of investigative cases relating to the illegal possession of illicit drugs is heavily dependent on test results which provide scientific evidence that the suspected person is in possession of the drug in question. Colour spot tests, more commonly referred to as presumptive tests, are useful in providing rapid qualitative identification that a controlled drug may be present in a sample, enabling prompt action at the point of seizure [1–3]. The production, consumption and commercialization of illicit substances remain a serious concern in most countries. Within the context of production and exploitation, amphetamine-type stimulants (ATS) such as methamphetamine (MAMP) and amphetamine (AMP) dominate the illicit drug market in many countries [4] where the amount of confiscated ATS has drastically increased in recent years [5–7].

Colorimetric spot test such as the Marquis, Simon's and Mandelin

tests are the 'gold' standard test used in ATS presumptive analysis. However, despite their wide-spread use in forensic analysis, there have been several reports of false positive results generated from chemical analysis of everyday items such as Epsom salts [8] and Krispy Kreme crumbs [9]. The limitation of colour spot test was recently brought to light in a case where unknown heart-shaped drugs were seized in Italy and presumptively identified as ATS using the Marquis reagent. However, further confirmatory test unraveled the substances as containing methyltestosterone, methanedone and androgen steroids with no trace of ATS being present [10,11]. Poor sensitivity of the colorimetric test when there are low levels of target analogue may be a significant contributing factor to false negative results [12]. In addition, the handling of colour spot reagents also poses increased health risk as many of the chemicals being used are highly corrosive and toxic. There is therefore an increased interest in the development of highly selective, ultrasensitive, rapid and safe-to-use colour spot test for accurate on-site

\* Corresponding author.

E-mail address: [o.adegoke@dundee.ac.uk](mailto:o.adegoke@dundee.ac.uk) (O. Adegoke).

and point of seizure ATS detection and one avenue of exploration to address this lies in the use of nanotechnology-based biosensors.

Over the last decade, nanomaterials-based artificial enzymes, known as nanozymes have emerged as a powerful alternative to natural enzymes in various applications ranging from pollutant removal, stem cell growth, cancer diagnostics and biosensing [13–15]. In the field of biosensing particularly, nanozyme-based peroxidase mimics involving the use of carbon-based nanomaterials [16–19], magnetic Fe<sub>3</sub>O<sub>4</sub> nanoparticles (MNPs) [19] and plasmonic nanoparticles NPs [20] as catalyst to catalyse the oxidation of a suitable substrate in the presence of hydrogen peroxide (H<sub>2</sub>O<sub>2</sub>) have been exploited in several colorimetric assays [21–23]. Gold NPs (AuNPs), characterized by their surface plasmon resonance (SPR) absorption feature are known to change colour relative to their chemical state and this property has been exploited in colorimetric assays [24]. Graphene oxide (GO) on the other hand, is a water-soluble 2D carbon nanomaterial, characterized by sheets of arranged carbon atoms in a honeycomb-like lattice structure and characterized by oxygen functional moieties (e.g. epoxy, carbonyl, carboxyl and hydroxyl) [25]. Despite the peroxidase mimic activity of AuNPs and graphene, their catalytic efficiency in sensor technology can be enhanced further by forming hybrid nanostructures [26,27]. Additionally, the incorporation of hemin (iron protoporphyrin IX) in a peroxidase mimic assay can also aid catalytic enhancement of the sensor. Hemin, known as the active site in heme-containing protein such as peroxidase, myoglobin, hemoglobin and catalases [28], exhibits peroxidase-like catalytic activity through the oxidation of a suitable substrate by H<sub>2</sub>O<sub>2</sub> [29].

To selectively target the analyte of interest, the incorporation of a receptor molecule within a nanozyme peroxidase mimic assay is an efficient way to achieve this. Aptamers are short single-stranded RNA or DNA sequences, capable of undergoing selective antigen interaction due to three-dimensional structure formation [30]. Intermolecular interaction with the target of interest via aromatic ring stacking, hydrogen bonding or van der Waal forces is facilitated by the nucleic acid aptamer structure (which could be a loop, quadruplex motifs, pseudoknot or k-turn) [31]. Compared with traditional antibodies, aptamers exhibit greater thermal stability, longer shelf-lives with no loss of activity and can easily be transported and stored [32].

In this work, we report on a novel catalytic-enhanced peroxidase mimic biosensor for the colorimetric detection of AMP and MAMP using GO-multi-shaped cetyltrimethylammonium bromide (CTAB)-AuNPs hybrid nanozyme with DNA aptamer as a bioreceptor and hemin as a catalytic signal amplifier. GO was first bound to CTAB-AuNPs via electrostatic interaction to form a GO-CTAB-AuNP hybrid nanozyme complex. Then a DNA aptamer, specific to the target ATS was thereafter bound to the GO-CTAB-AuNP hybrid nanozyme surface to capture the target ATS. This was followed by the binding of hemin and the subsequent catalytic oxidation of 3,3',5,5'-tetramethylbenzidine (TMB) by H<sub>2</sub>O<sub>2</sub> to generate a deep blue colour specific to the target ATS. To the best of our knowledge, the aptamer-based GO-CTAB-AuNP-hemin peroxidase mimic biosensor for ATS is the first of its kind and can colorimetrically detect AMP and MAMP as individual compounds in ~1 minute (min) with high sensitivity and selectivity.

## 2. Experimental

### 2.1. Materials

± Methadone HCl (≥98%), acetylsalicylic acid, acetaminophen, silver nitrate (AgNO<sub>3</sub>), (+) MAMP hydrochloride, d-AMP, BIS-TRIS, Trizma® acetate and H<sub>2</sub>O<sub>2</sub> (30% w/w) in solution with stabilizer were purchased from Sigma Aldrich. Tris(hydroxymethyl)aminomethane was purchased from Formedium. Dimethyl sulfoxide (DMSO), ascorbic acid, TMB, MES, CTAB, potassium acetate (KAc) and gold (III) chloride trihydrate (HAuCl<sub>4</sub>·3H<sub>2</sub>O), graphite powder and potassium permanganate (KMnO<sub>4</sub>) were purchased from Thermo Fisher. 3,6-

Diacetylmorphine and codeine HCl were purchased from lipomed. The thiolated DNA aptamer oligonucleotide: The AMP and MAMP-specific DNA aptamer with the nucleic acid sequence;

HSC<sub>6</sub>-5'-ACGGTTGCAAGTGGGACTCTGGTAGGCTGGGTAATTTGG [33] was synthesized and purified by Eurofins. All other chemicals were used as received. The buffer solution used in this study was prepared in Milli-Q water.

### 2.2. Characterization

UV/vis absorption measurements were carried out on a Cary Eclipse (Varian) spectrophotometer. Transmission electron microscopy (TEM) measurements were performed on a JEOL JEM-1200EX operated at 80 kV. Scanning electron microscope (SEM) imaging was carried out using a JEOL JSM 7400F field emission SEM. Zeta potential measurements were carried out using a Brookhaven Nanobrook Omni particle size and zeta potential analyser. Absorbance measurements were recorded on an 800 TS microplate absorbance reader from BioTek. The Raman spectra were collected using an in-house built microprobe system equipped with a continuous wave laser sources emitting at 633 nm, the Oriel MS257 monochromator fitted with the Andor Newton EMCCD detector TE cooled to -70 °C. The backscattering configuration was used for the signal collection. The incident power on the samples was 7 mW. The spectra were recorded using a 40× objective, a 1 s accumulation time with a total of 10 accumulations.

### 2.3. Synthesis of multi-shape CTAB-AuNPs

Multi-shape CTAB-AuNPs were synthesized via the seed-mediated approach with modifications [34]. The seed solution was prepared by mixing 10 mL 0.1 M CTAB, 5 mL 2.5 × 10<sup>-4</sup> M HAuCl<sub>4</sub>·3H<sub>2</sub>O and 0.6 mL 0.01 M NaBH<sub>4</sub>. Thereafter, 150 µL of the seed solution was added into the growth solution containing a mixture of 10 mL 0.1 M CTAB, 0.4 mL 0.1 M ascorbic acid, 0.5 mL 0.004 M AgNO<sub>3</sub> and 5 mL 2.5 × 10<sup>-4</sup> M HAuCl<sub>4</sub>·3H<sub>2</sub>O. The solution was stirred for few min and kept in the dark for ~24 hours. Purification of the NPs was carried out via centrifugation.

### 2.4. Synthesis of GO nanosheets

GO nanosheets were synthesized via the modified Hummers method [35,36]. Graphite oxide was firstly prepared by mixing 2.5 g graphite powder and 1.25 g NaNO<sub>3</sub> in ice-cooled solution of 60 mL H<sub>2</sub>SO<sub>4</sub>. Once the graphite powder was thoroughly dispersed in the acidified solution, 7.5 g KMnO<sub>4</sub> was added and the solution was kept in ice for ~2 h and subsequently stirred for ~24 h at room temperature. The reaction mixture was then placed in an ice bath and 75 mL of Milli-Q water was added slowly. The reaction mixture was thereafter stirred for ~24 h at ~100 °C and allowed to cool down prior to the slow addition of 25 mL 35% H<sub>2</sub>O<sub>2</sub>. Graphite oxide was thereafter purified by centrifugation with 5% HCl followed by acetone and dried in the fume hood. Graphite oxide was exfoliated to GO via ultrasonication.

### 2.5. Bioassay procedure

NaAc-KAc-KCl-HCl is a novel buffer solution developed in this work and was used as the choice buffer for the ATS catalytic assay. It was prepared by mixing 0.25 g NaAc, 0.25 g KAc, and 0.37 g KCl in 50 mL of MilliQ water. Then, 6.7 mL 0.1 M HCl was added into the 50 mL buffer solution and made up to 100 mL with MilliQ water and the pH of the solution was adjusted to 2.2. Electrostatic interaction between GO nanosheets and CTAB-AuNPs was formed by mixing 0.2 mg/mL GO with 0.04 nM CTAB-AuNPs. The final concentration of the GO-CTAB-AuNP hybrid was 0.03 nM. Thereafter, 40 µL of GO-CTAB-AuNP hybrid solution was mixed with 5 µL DNA aptamer (100 µM), 150 µL of target ATS concentration in KCl-HCl-NaAc-KAc buffer, pH 2.2, 5 µL hemin

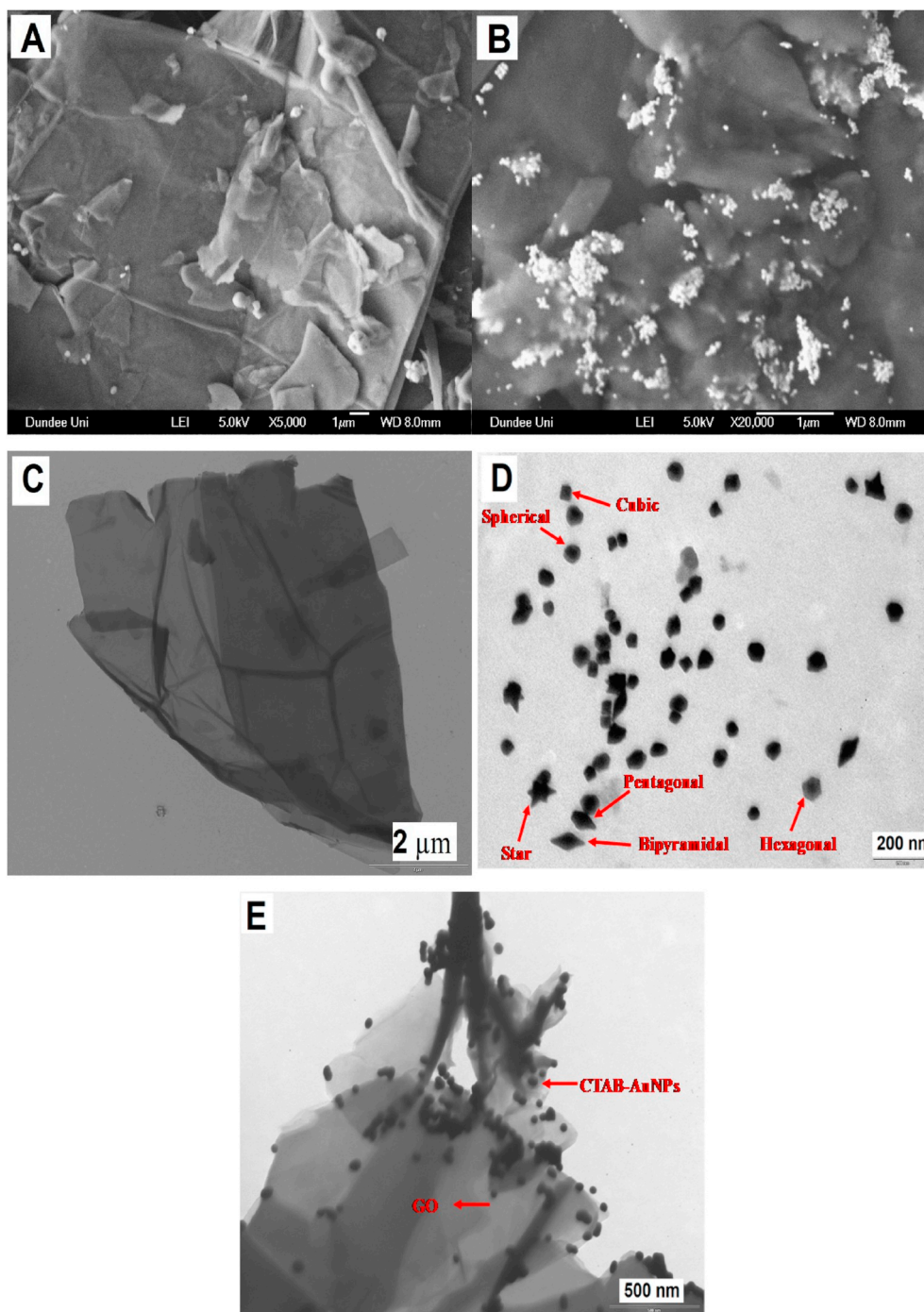


**Fig. 1.** SEM images of (A) GO and (B) GO-AuNP nanohybrid. TEM images of (C) GO, (D) CTAB-AuNPs and (E) GO-AuNP nanohybrid.

(100  $\mu\text{M}$ ), 90  $\mu\text{L}$  TMB (3000  $\mu\text{M}$ ) and 60  $\mu\text{L}$   $\text{H}_2\text{O}_2$  (1.2 M) in a 96-well plate. The absorbance of the solution was recorded at  $\sim 1$  min after adding  $\text{H}_2\text{O}_2$  using a BioTek 800 TS microplate reader with a 630 nm filter.

### 3. Results and discussion

#### 3.1. Structural properties

##### 3.1.1. SEM analysis

Graphene, known to be conceptually flat, is characterized by an  $\text{sp}^2$  trigonal-bonded hybridized array of carbon atom sheets. It is typically synthesized by chemical exfoliation of graphite oxide under strong

oxidative and acidic reaction conditions and is characterized by oxygen atoms that are embedded in functional groups such as carboxyls, hydroxyls, epoxides and esters which lie both on the graphene sheet edges and on the basal plane [37,38]. GO is stabilized as a colloidal solution in water and is rendered negatively charged when the groups at the sheet edges, particularly carboxyl groups are ionized [37]. Fig. 1A and B shows the SEM images of GO and GO-CTAB-AuNP nanohybrid. From Fig. 1A, GO is characterized by crumpled thin and randomly aggregated flaky sheets, stacked together with observed folding and wrinkles. The corresponding GO-CTAB-AuNP nanohybrid SEM image shown in Fig. 1B, revealed the retained morphology of GO and the embedded CTAB-AuNPs across the surface sheet.

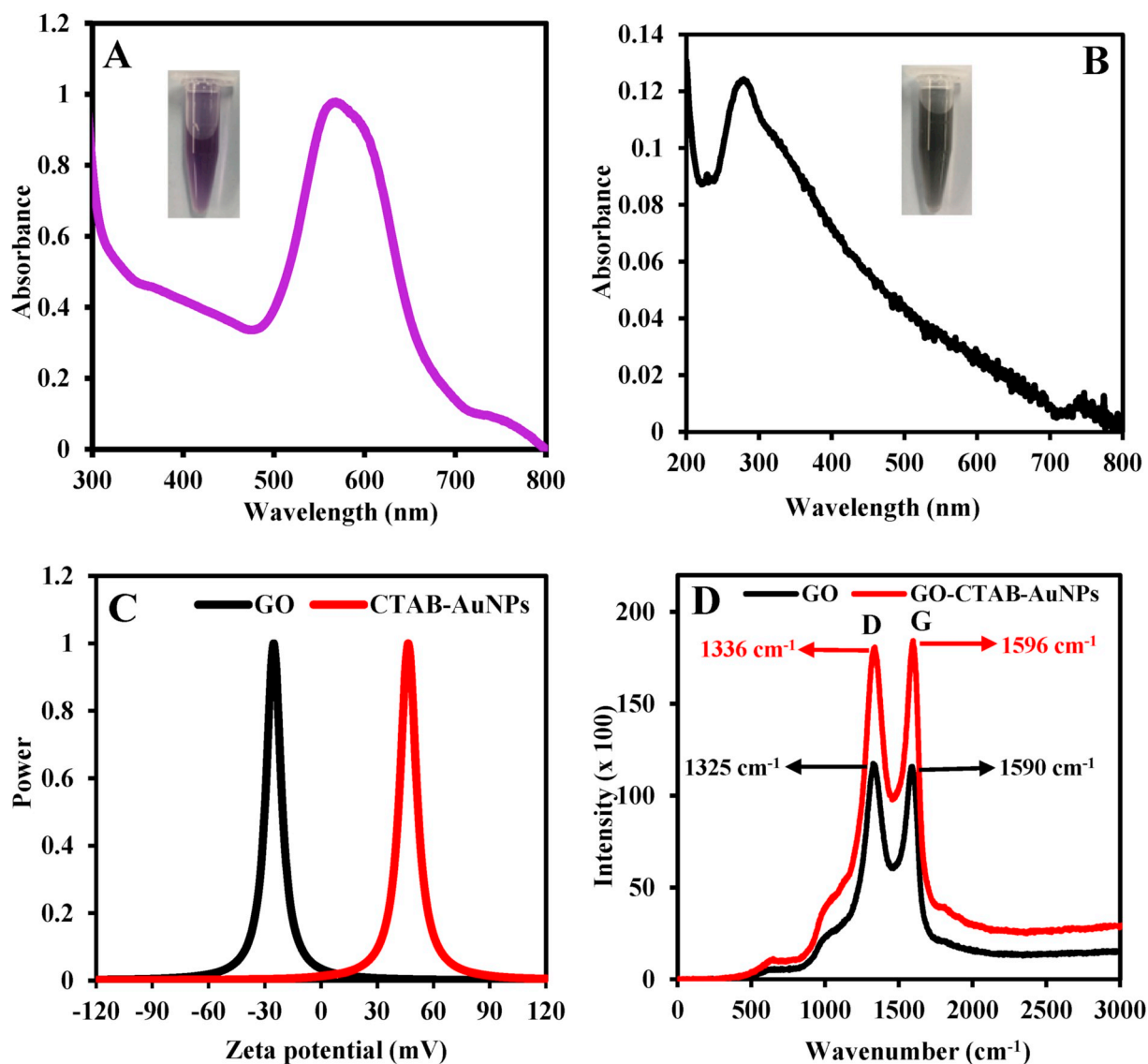


Fig. 2. UV/vis absorption spectra of (A) multi-shaped CTAB-AuNPs and (B) GO nanosheet. ZP curve (C) and Raman spectra (D) of GO and CTAB-AuNPs. Inset of Fig. 2B = picture of CTAB-AuNPs in solution and inset of Fig. 2C = picture of GO in solution.

### 3.1.2. TEM analysis

TEM analysis was used to further probe the surface morphology of GO, GO-CTAB-AuNP nanohybrid and the positively charged CTAB-AuNPs. Fig. 1C shows that the TEM micrograph of GO is characterized by well-exfoliated individual sheets without the presence of bulk aggregates. The TEM image of the multi-shaped CTAB-AuNPs (Fig. 1D) synthesized via the seed-mediated approach, reveals a well-dispersed size distribution and homogeneity with a mixture of cubic, spherical, star, bipyramidal, hexagonal and irregular-shaped particles. The formation of various shaped particles is understood to arise from the interplay between the growth kinetics and the faceting properties of the CTAB surfactant [34]. The average particle size of CTAB-AuNPs was 47 nm. The corresponding TEM image of GO-CTAB-AuNP is shown in Fig. 1E. From the TEM micrograph, anchored CTAB-AuNPs were seen embedded within the sheet layer of GO, thus revealing the strong binding interaction between GO and CTAB-AuNPs.

## 3.2. Optical properties

### 3.2.1. UV/vis absorption

The optical properties of AuNPs are known to be determined by the

presence of SPR absorption band. Any change in the geometry, shape or size of the particles influences the local electron confinement, resulting in alterations of the SPR band position and consequently the colour change of the colloidal solution [39,40]. Fig. 2A shows that the multi-shaped CTAB-AuNPs solution is characterized by a distinctive SPR absorption band peaked at ~570 nm. Due to the altered shape of the NPs, the SPR band of the synthesized colloidal solution appears to be red-shifted compared with that of Au nanospheres (peaked at a wavelength of ~520 nm) and blue-shifted to that of anisotropic Au nanorods (> 600 nm) [41]. The inset of Fig. 2A shows the strong purple colloidal solution of the synthesized CTAB-AuNPs. For GO (Fig. 2B), the characteristic sharp absorption peak at ~279 nm is assigned to the  $\pi \rightarrow \pi^*$  transition of the  $sp^2$  C=C bond [42] while the broad peak shoulder at ~310–380 nm is assigned to the  $n \rightarrow \pi^*$  transition of the C-O-C (epoxide) and R-O-O-R (peroxide) functional moieties [43].

### 3.2.2. Zeta potential

The amount of work needed to move a unit positive charge (without acceleration) with affinity to the NP surface is reflected in the electric field potential. The electric field potential of a colloidal NP solution at the slipping/shear plane of an applied electric field is known as the Zeta

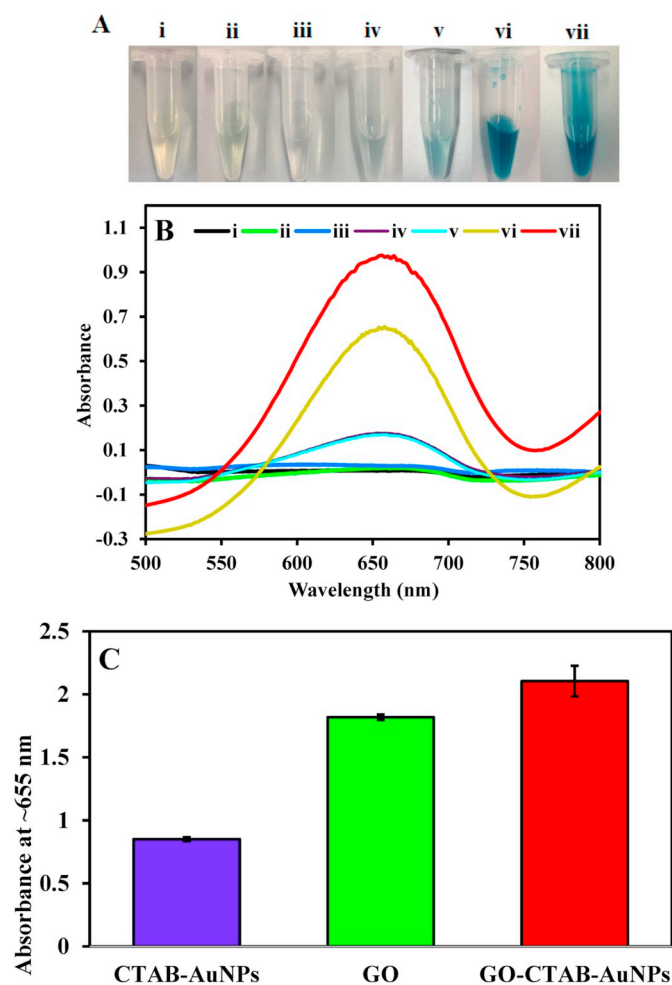


**Fig. 3.** (A) Photographic colorimetric picture and (B) corresponding UV/vis absorption spectra of (i) TMB/H<sub>2</sub>O<sub>2</sub>, (ii) GO-AuNPs + TMB/H<sub>2</sub>O<sub>2</sub>, (iii) GO-AuNPs + AMP, (iv) GO-AuNPs + DNA aptamer + AMP + TMB/H<sub>2</sub>O<sub>2</sub>, (v) GO-AuNPs + DNA aptamer + MAMP + TMB/H<sub>2</sub>O<sub>2</sub>, (vi) GO-AuNPs + DNA aptamer + AMP + hemin + TMB/H<sub>2</sub>O<sub>2</sub> and (vii) GO-AuNPs + DNA aptamer + MAMP + hemin + TMB/H<sub>2</sub>O<sub>2</sub>. (C) Enhanced catalytic signal of the GO-CTAB-AuNP hybrid to MAMP detection in comparison to CTAB-AuNPs and GO. [ATS] = 100 μM. Reaction carried out at room temperature.

potential. The adsorbed double layer, known as the electric double layer (EDL) is created on the NP surface when the colloidal NP solution is dispersed in solution. The EDL inner layer is embedded with ions/molecules having opposite charge to the colloidal NP solution. Therefore, the principle of Zeta potential relates to the difference in the electric field potential between the surrounding layer of dispersant and the EDL of an electrophoretic mobile particle [44]. The Zeta potential of GO and CTAB-AuNPs were measured to confirm the surface charge of the respective nanomaterials. From Fig. 2C, the Zeta potential curves reveal the negative charge potential of GO with a Zeta potential charge of -27.61 mV and the positive charge potential of CTAB-AuNPs with a Zeta potential charge of +46.49 mV.

### 3.2.3. Raman analysis

The Raman spectra of GO and GO-CTAB-AuNP shown in Fig. 2D are characterized by two distinct bands known as the D and G band [45]. For GO, the peak at 1325 cm<sup>-1</sup> is ascribed to the D band and it arises due to the reduction in size of the sp<sup>2</sup> domain plain induced from strong oxidation of graphene nanosheets. The second peak at 1590 cm<sup>-1</sup> is ascribed to the G band and it arises from the E<sub>2g</sub> first-order scattering [45]. An increase in intensity and a slight shift of the D (1336 cm<sup>-1</sup>) and G band (1596 cm<sup>-1</sup>) to higher wavenumbers was observed for the

GO-CTAB-AuNP nano hybrid relative to GO. The observed change can be attributed to the electrostatic binding interaction between GO and CTAB-AuNPs. Prior to the electrostatic binding interaction, the intensity ratio (I<sub>D</sub>/I<sub>G</sub>) for GO was 1.01 but decreased slightly to 0.98 for the GO-CTAB-AuNP nano hybrid.

### 3.3. Catalytic activity

The peroxidase mimic activity of the aptamer-based GO-CTAB-AuNP-hemin biosensor in inducing a catalytic colour reaction for the target ATS was investigated. From the UV/vis absorption data (Fig. 3A and B), no catalytic response and visible colour change was observed for TMB/H<sub>2</sub>O<sub>2</sub>, GO-CTAB-AuNP + TMB/H<sub>2</sub>O<sub>2</sub> and GO-CTAB-AuNP + AMP. However, we observed a weak catalytic response when the GO-CTAB-AuNP hybrid nanozyme was reacted with the DNA aptamer, target ATS and TMB/H<sub>2</sub>O<sub>2</sub> but without the catalytic amplifying effect of hemin in the biosensor system. With hemin incorporated into the catalytic biosensor system, a strong catalytic signal and blue colorimetric reaction, characterized by a distinct absorption peak at ~660 nm, was observed for both AMP and MAMP. It is evident that the strong colorimetric and corresponding catalytic response can be attributed to the signal-enhancing effect of hemin in the biosensor system.

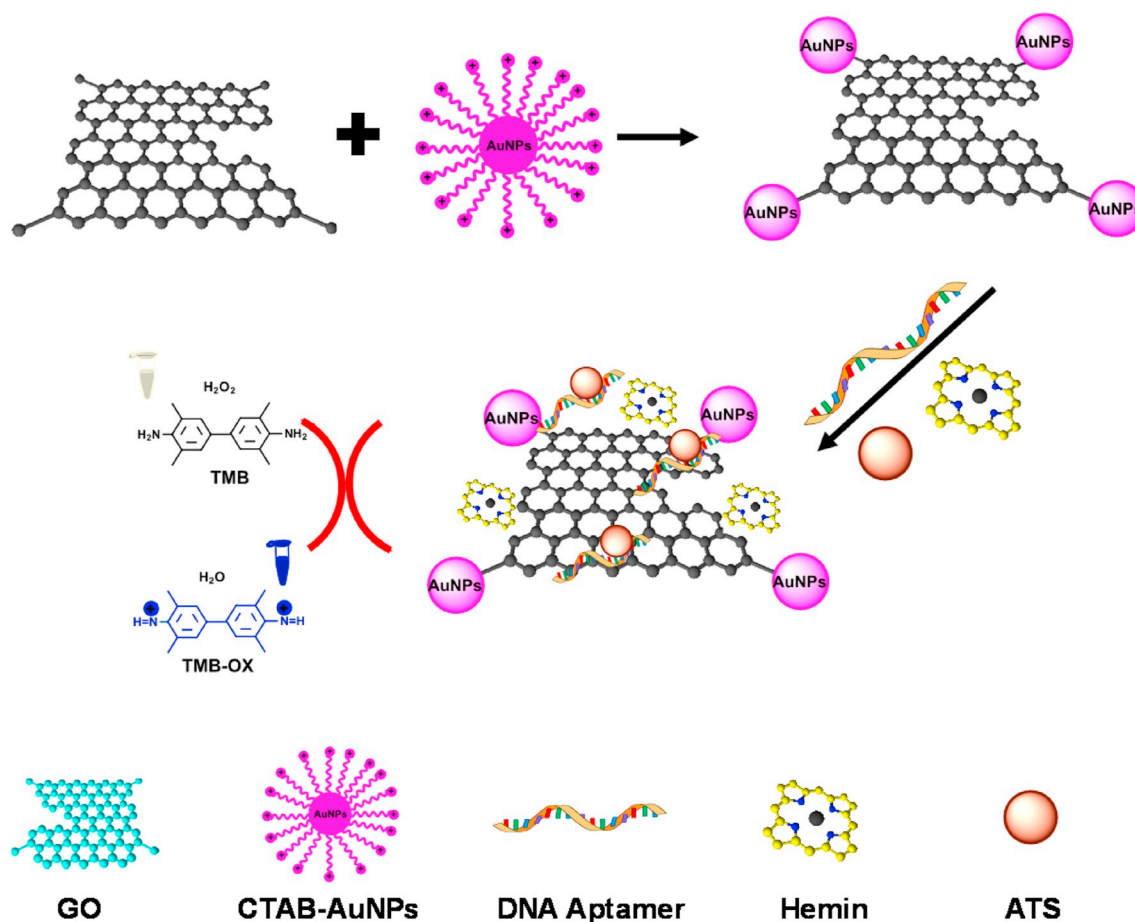
To confirm the catalytic-enhancing property of the hybrid nanozyme, the catalytic signal of GO, CTAB-AuNPs and the GO-CTAB-AuNP hybrid nanozyme to MAMP detection was investigated under the same experimental condition. Fig. 3C shows that the GO-CTAB-AuNPs hybrid nanozyme induced higher catalytic signal for the detection of MAMP in comparison to the signal obtained for GO and CTAB-AuNPs. From the data, it is tentative that the combined catalytic activity of GO and CTAB-AuNPs, embedded within the hybrid nanozyme system, induced the enhanced catalytic signal. Thus, the sensitivity of the biosensor to MAMP detection was enhanced when GO-CTAB-AuNPs hybrid was used as the nanozyme catalyst.

The working principle of the aptamer-based GO-CTAB-AuNP-hemin peroxidase mimic catalytic biosensor for ATS detection is presented in Scheme 1. In general, peroxide-like activity of nanozymes using DNA aptamers as affinity receptors have been reported by several groups [46–49]. The mechanism of peroxidase-like catalytic activity of nanozymes have generally been attributed to the decomposition of H<sub>2</sub>O<sub>2</sub> to hydroxyl radicals by the nanozyme catalyst [25]. Firstly, negatively charged GO is bound to the positively charged CTAB-AuNPs via electrostatic interaction. Thereafter, a thiolated DNA aptamer specific to the target ATS was adsorbed onto the GO-CTAB-AuNP surface via either DNA base stacking with GO hydrophobic domains, electrostatic repulsion with GO oxygen-rich domains or hydrogen bonding. Studies have also shown that the pyrimidine bases (C and T) bind more strongly to GO than the purine bases (G and A), suggesting the possibility that aromatic-based stacking interactions can occur with the bonded GO [50]. To enhance the binding interaction, the DNA aptamer was thiolated to provide the possibility of additional adsorption binding to the CTAB-AuNP surface. The target ATS drug was then added to the biosensor system and captured by the DNA aptamer followed swiftly by the addition of hemin. Hemin binds strongly to graphene via π-π interaction and was used to enhance the catalytic signal of the biosensor. TMB was then added into the aptamer-GO-CTAB-AuNP-hemin system and thereafter catalyzed the oxidation of the hybrid nanozyme in the presence of H<sub>2</sub>O<sub>2</sub>, leading to the generation of colored blue product that corresponds selectively to the concentration of the detected ATS drug.

### 3.4. Optimization

#### 3.4.1. Buffer and pH effect

pH stabilization during enzymatic assays can be accomplished with a buffer solution while the buffer components can influence optimum catalytic efficiency. The term “Good buffers” was coined to represent



**Scheme 1.** Schematic representation of the hybrid nanozyme peroxidase mimic aptamer-based biosensor for ATS detection. GO is first bound to CTAB-AuNP via electrostatic interaction to form a GO-AuNP hybrid nanozyme complex. Thereafter, the DNA aptamer is bound to the GO-AuNP hybrid nanozyme and captures the target ATS. Hemin is added to the system to enhance the catalytic signal followed by the catalytic oxidation of TMB by H<sub>2</sub>O<sub>2</sub>, generating a blue colour complex specific to the target ATS concentration.

certain buffers which demonstrated a catalytic stabilizing effect on the enzymatic assay [51]. Finding the appropriate buffer for optimum catalytic efficiency is quite challenging due to the varying degree of analyte interactions for each enzyme assay. To find the appropriate buffer for the targeted ATS detection, we probed the catalytic sensitivity of the aptamer-based GO-CTAB-AuNP-hemin hybrid biosensor in the presence of five different buffer solutions (Fig. 4A). From our investigation, we found that NaAc-KAc-KCl-HCl, pH 2.2 buffer, a novel buffer developed in this work, induced an optimum catalytic signal for AMP and MAMP detection. Hence, this buffer was chosen as the buffer of choice for the ATS catalytic peroxidase mimic assay.

Subsequently, the effect of pH on the catalytic response of the peroxidase mimic biosensor to AMP and MAMP detection was studied. Fig. 4B shows the catalytic response of the aptamer-based GO-CTAB-AuNP-hemin hybrid biosensor to AMP and MAMP in the pH range 2.2–5.0. From the data, optimum catalytic response was observed at pH 2.2, this then decreased at pH 2.6 and increased steadily to pH 3.8 for MAMP and pH 4.0 for AMP and finally, the catalytic response decreased steadily up until pH 5.0. Based on the observed data, pH 2.2 was chosen as the optimum pH condition for the catalytic assay.

#### 3.4.2. Effects of GO and CTAB-AuNPs concentration

The effect of GO concentration on the catalytic efficiency of the aptamer-based GO-CTAB-AuNP-hemin peroxidase mimic biosensor for AMP and MAMP detection was studied. Fig. 5A shows the catalytic response obtained for AMP and MAMP detection at different GO concentration. From the data, we observe a slight decrease in catalytic

signal relative to increasing concentration of GO. The absorption spectra showing the effect of GO on the SPR absorption peak of CTAB-AuNPs was also studied. As shown in Fig. S1, we found the intensity of the SPR absorption peak decreased as the concentration of GO increased. Based on these results, we chose 0.2 mg/mL GO as the choice concentration for the peroxidase mimic assay.

The effects of CTAB-AuNPs on the catalytic efficiency of the peroxidase mimic assay was also studied using AMP as the target drug. From Fig. S2A, we observe that the catalytic signal of the peroxidase mimic biosensor increased as the concentration of CTAB-AuNPs increased. The absorption spectra (Fig. S2B) also showed that the SPR absorption peak was influenced by the plasmonic NP concentration. From the observed data, we chose 0.04 nM CTAB-AuNPs as the choice concentration for the peroxidase mimic assay.

#### 3.4.3. Effects of hemin concentration

Hemin was used as a catalytic signal enhancer for the peroxidase mimic biosensor. Hence, the effects of hemin concentration on the aptamer-based GO-CTAB-AuNP-hemin peroxidase mimic biosensor for AMP and MAMP detection was studied. A steady increase in catalytic signal was observed with increasing hemin concentration for AMP and MAMP detection as shown in Fig. 5B. Hence, 100  $\mu$ M hemin was chosen as the optimum concentration for enhanced catalytic reaction.

#### 3.4.4. Effects of TMB and H<sub>2</sub>O<sub>2</sub> concentration

The effects of TMB and H<sub>2</sub>O<sub>2</sub> concentration on the aptamer-based GO-CTAB-AuNP-hemin peroxidase mimic biosensor was studied. The

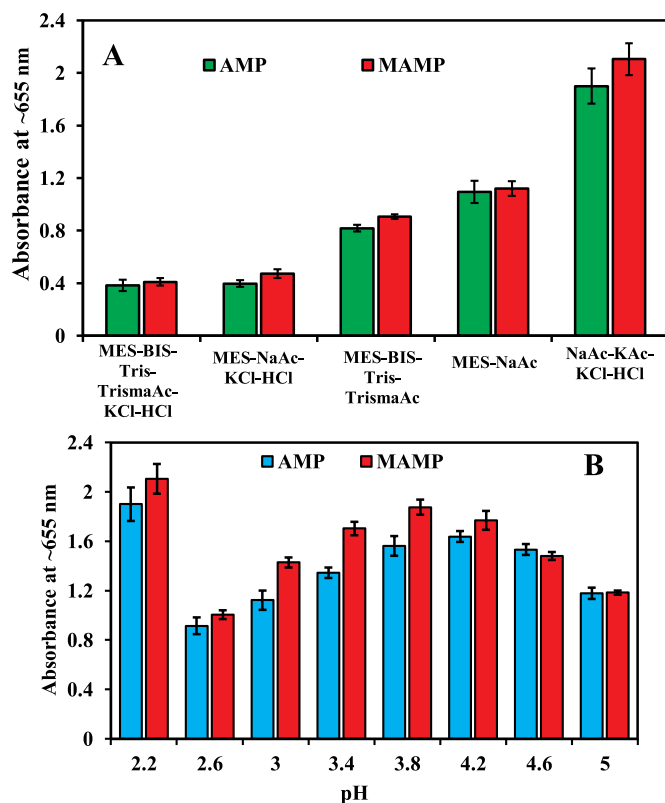


Fig. 4. Catalytic response of the aptamer-based GO-CTAB-AuNP-hemin hybrid nanozyme to AMP and MAMP detection in different buffer solutions (A) and at different pH conditions (buffer: NaAc-KAc-KCl-HCl, pH 2.2) (B). GO-CTAB-AuNP hybrid nanozyme (0.03 nM); 100  $\mu$ M DNA aptamer; 100  $\mu$ M ATS; 100  $\mu$ M hemin; 3000  $\mu$ M TMB; 1.2 M  $H_2O_2$ .

catalytic signal to MAMP detection was probed in the presence of TMB concentration from 250 to 3000  $\mu$ M and  $H_2O_2$  concentration from 0.2 to 1.2 M. As shown in Fig. 5C and D, the catalytic absorption peak at around 660 nm, increased steadily as the concentration of TMB and  $H_2O_2$  increased in the biosensor system. We observed a higher margin of difference in catalytic signal for increasing concentration of  $H_2O_2$  than for TMB. This indicates that an increasing concentration of  $H_2O_2$  had a more significant impact on the catalytic signal of the peroxidase mimic biosensor than an increasing concentration of TMB. Based on the observed results, 3000  $\mu$ M TMB and 1.2 M  $H_2O_2$  were chosen as the optimum substrate and oxidant concentrations for the peroxidase mimic biosensor.

### 3.5. Nanozyme kinetic bioassay

Kinetic studies of the aptamer-based GO-CTAB-AuNP-hemin peroxidase mimic biosensor was carried out to reveal changes in the velocity of the reaction as a function of changes in the substrate concentration at a fixed enzyme concentration [52]. Firstly, the absorbance vs time plots for varying TMB substrate concentration (fixed  $H_2O_2$  concentration) and  $H_2O_2$  concentration (fixed TMB concentration), were used to determine the initial rate of reaction ( $v$ ) (i.e., the slope of the graph), the value of  $v$  was then divided by the extinction coefficient of TMB ( $3.9 \times 10^4 \text{ M}^{-1} \text{ cm}^{-1}$ ) [53]. The Michaelis-Menten nonlinear curve was obtained according to equation (1) by plotting  $v$  vs varying concentration of TMB (fixed  $H_2O_2$  concentration) (Fig. S3A) and  $H_2O_2$  (fixed TMB concentration) (Fig. S3C):

$$v = \frac{V_{max} \cdot [S]}{[S] + K_m} \quad (1)$$

The linear curve was fitted by plotting  $\frac{1}{v}$  versus (Figs. S3B and D)

according to the Lineweaver-Burke equation [52]:

$$\frac{1}{v} = \frac{K_m}{V_{max} \cdot [S]} + \frac{1}{V_{max}} \quad (2)$$

$V_{max}$  is the maximum reaction velocity,  $K_m$  is the Michaelis-Menten constant and  $[S]$  is the substrate concentration. The intercept of the plot is equal to  $\frac{1}{V_{max}}$  and was used to determine the value of  $V_{max}$  while  $K_m$  was determined by multiplying the slope value with  $V_{max}$ .

Table 1 shows the  $V_{max}$ ,  $K_m$  and  $K_{cat}$  values obtained for MAMP and AMP detection in the presence of TMB and  $H_2O_2$ .  $K_m$  is the measure of catalytic affinity between the hybrid nanozyme and substrate in which a low  $K_m$  value represents a strong affinity and vice versa;  $V_{max}$  is a measure of the catalytic rate of reaction in which a higher  $V_{max}$  value represents a higher catalytic rate of reaction;  $K_{cat}$  is the catalytic constant whose value relates to the maximum number of colored products (oxidized substrate) "turned over" per nanozyme per second ( $K_{cat} = V_{max}/[E]$ , where E is the hybrid nanozyme concentration. From the kinetic assay results (Table 1), we observed a stronger affinity between the hybrid nanozyme and the substrate (TMB) for AMP detection based on the lower  $K_m$  value (0.24 mM) obtained compared to MAMP ( $K_m = 0.52 \text{ mM}$ ). However, the higher  $K_{cat}$  value obtained for MAMP detection ( $K_{cat} = 8.2 \times 10^5 \text{ s}^{-1}$ ) in the presence of TMB substrate, suggests there was higher amount of oxidized substrate generated per nanozyme per second relative to AMP ( $K_{cat} = 2.7 \times 10^5 \text{ s}^{-1}$ ). Generally, we observed a higher  $K_{cat}$  value for MAMP detection relative to AMP in the presence of both TMB and  $H_2O_2$ . Our work is the first to report on the  $K_m$ ,  $V_{max}$  and  $K_{cat}$  values for enzymatic catalytic reaction of MAMP and AMP using the novel GO-CTAB-AuNP-hemin hybrid nanozyme.

### 3.6. Quantitative detection of AMP and MAMP

Quantitative detection of AMP and MAMP using the aptamer-based GO-CTAB-AuNP-hemin peroxidase mimic biosensor was carried out in the concentration range of 0.5–100  $\mu$ M. Fig. 6A shows the quantitative colorimetric response of 0.5–100  $\mu$ M AMP and MAMP detection using the peroxidase mimic biosensor. From the colour reaction, we observed a clear change in the colour intensity as the detected concentration of AMP increased. Whereas for MAMP, the intensity of the colour reaction was less prominent but clearly distinguishable in the catalytic signal. The difference may be attributed to the very strong oxidation of TMB in the presence of MAMP. From Table 1, we observed that the  $K_{cat}$  value for MAMP in the presence of the substrate TMB and  $H_2O_2$  was higher than the value obtained for AMP. This proves to show that the aptamer-based GO-CTAB-AuNP-hemin peroxidase mimic biosensor exhibits higher catalytic activity to MAMP than AMP.

The corresponding catalytic signal curve shown in Fig. 6B for AMP and Fig. 6C for MAMP revealed quantitative detection of the drug sample. As the concentration of the target ATS increased in the detection system, the catalytic signal progressively increased. From the linear calibration curve, we determined the limit of detection (LOD) by multiplying the standard deviation of blank measurement by 3 and dividing by the slope of the linear calibration graph. The LOD obtained for AMP detection was 185 nM (34.1 ng/mL) and 154 nM (28.6 ng/mL) for MAMP detection. Table 2 shows the improved sensitivity of the peroxidase mimic biosensor over most published colorimetric data for AMP and MAMP detection. From the comparison (Table 2), the response time (~1 min) of our peroxidase mimic biosensor is the best reported to date.

### 3.7. Detection and quantitation of AMP in a seized sample

The efficacy of the aptamer-based GO-CTAB-AuNP-hemin peroxidase mimic biosensor was probed for the detection and quantitation of AMP in a seized drug sample. Fig. S4A shows the colorimetric response of the peroxidase mimic biosensor to different AMP concentrations within the sample. It is evident that the colour intensity increased steadily as the concentration of AMP increased. The corresponding

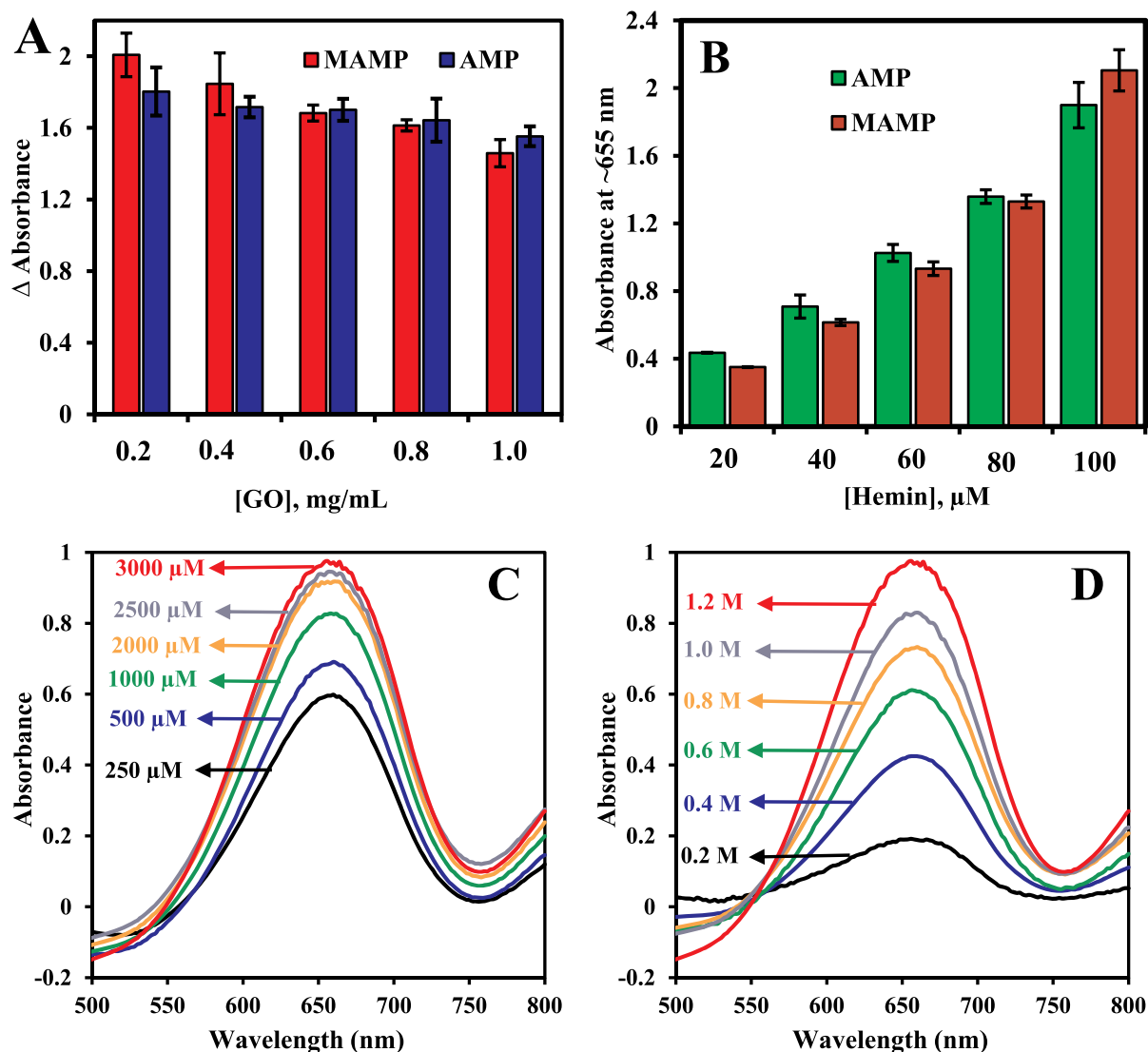


**Fig. 5.** Catalytic response of the aptamer-based GO-AuNP-hemin peroxidase mimic biosensor to MAMP and AMP detection at different (A) GO and (B) hemin concentrations. UV/vis absorption spectra showing the catalytic response of the peroxidase mimic biosensor to MAMP detection at different (C) TMB concentration ( $\text{H}_2\text{O}_2$  concentration fixed) and (D)  $\text{H}_2\text{O}_2$  concentration (TMB concentration fixed). GO-CTAB-AuNP hybrid nanozyme (0.03 nM); 100  $\mu\text{M}$  DNA aptamer; 100  $\mu\text{M}$  ATS; 100  $\mu\text{M}$  hemin; 3000  $\mu\text{M}$  TMB; 1.2 M  $\text{H}_2\text{O}_2$ .

**Table 1**

$K_m$ ,  $V_{\max}$  and  $K_{\text{cat}}$  kinetic parameters of GO-CTAB-AuNP hybrid nanozyme for MAMP and AMP detection.

Drug	[E] M	Substrate	$V_{\max}$ ( $\text{M s}^{-1}$ )	$K_m$ (mM)	$K_{\text{cat}}$ ( $\text{s}^{-1}$ )
MAMP	$2.7 \times 10^{-11}$	TMB	$2.2 \times 10^{-5}$	0.52	$8.2 \times 10^5$
MAMP	$2.7 \times 10^{-11}$	$\text{H}_2\text{O}_2$	$3.1 \times 10^{-5}$	1100	$1.2 \times 10^6$
AMP	$2.7 \times 10^{-11}$	TMB	$6.8 \times 10^{-6}$	0.24	$2.5 \times 10^5$
AMP	$2.7 \times 10^{-11}$	$\text{H}_2\text{O}_2$	$8.5 \times 10^{-6}$	396	$3.2 \times 10^5$

quantitative catalytic signal curve presented in Fig. S4B revealed the steady increase in catalytic signal as the concentration of AMP increased. From the catalytic signal plot, we determined the LOD to be 187 nM (34.5 ng/mL) which was close to the LOD obtained for standard AMP sample (185 nM (34.1 ng/mL)).

### 3.8. Selectivity of the peroxidase-mimic bioassay

Marquis, Simon's and Mandelin reagents are the standard presumptive tests used in ATS analysis. Marquis and Mandelin reagents are

specifically used for AMP and MAMP while Simon's reagent is used to differentiate between MAMP and AMP [54]. However, there are also several other substances that respond positively to both the Marquis and Mandelin reagents [55] and as such a more selective presumptive test designed specifically for AMP and MAMP would be very advantageous. To probe the selectivity of the peroxidase mimic biosensor to AMP and MAMP, known substances and drugs that respond positively to the Marquis and Mandelin reagents were tested. Table S1 provides information on the positive response of the tested drugs and substances to Marquis and Mandelin reagents and the colour they exhibit.

Fig. 7 shows the colorimetric response and catalytic signal obtained for AMP and MAMP in comparison to the data obtained for the tested substances and drugs. From the data, we observed a very strong catalytic signal for AMP and MAMP accompanied with a very deep blue colorimetric reaction. In contrast, a very weak catalytic response was exhibited by the additional tested substances and drugs which could be differentiated from the deep blue colour exhibited by AMP and MAMP. In terms of the catalytic signal efficiency, the AMP catalytic signal was 4-fold higher while MAMP was at most 5-fold higher than the catalytic signal obtained for the tested interferences. Based on our results, it is

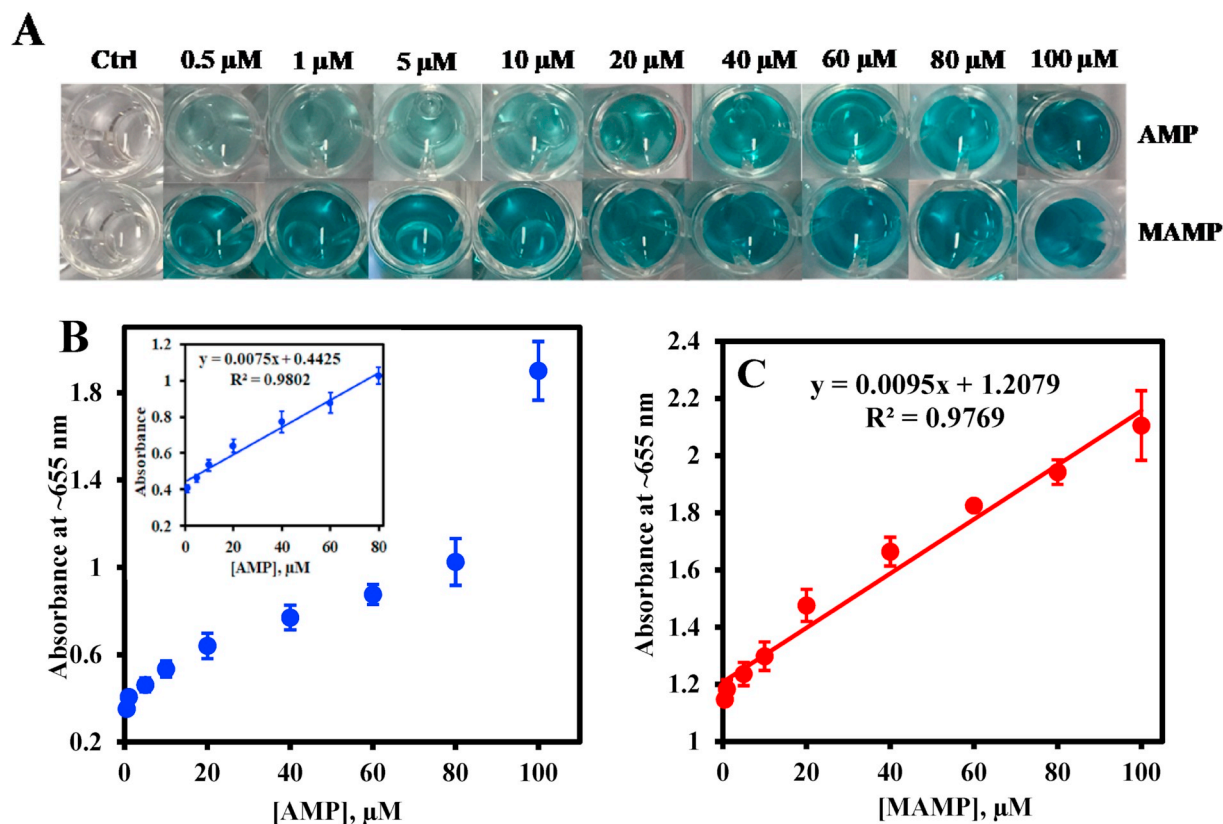


Fig. 6. Quantitative detection of the target AMP and MAMP. (A) Photographical colorimetric response and catalytic calibration plot for quantitative detection of AMP (B) and MAMP (C). Inset of Fig. 7B is the linear calibration curve for AMP detection. GO-CTAB-AuNP hybrid nanozyme (0.03 nM); 100  $\mu$ M DNA aptamer; 100  $\mu$ M ATS; 100  $\mu$ M hemin; 3000  $\mu$ M TMB; 1.2 M  $H_2O_2$ . Data recorded at  $\sim$ 1 min.

Table 2

Comparison of the analytical performance of the aptamer-GO-CTAB-AuNP-hemin hybrid nanozyme biosensor probe for ATS detection with published data.

Probe	Drug	Method	LOD	Detection time	Ref.
Solid PDMS-TEOS-SiO <sub>2</sub> matrix	AMP	Colorimetry	$5 \times 10^6$ ng/mL	10 min	[4]
	MAMP	Colorimetry	$4 \times 10^6$ ng/mL	10 min	
Au@Ag DNA aptamer probe	MAMP	Colorimetry	0.0149 ng/mL	15 min	[56]
Simons reagent in sol-gel matrix	MAMP	Colorimetry	$2.1 \times 10^5$ – $5.9 \times 10^5$ ng/mL	2 min	[57]
Centrifugal microdevice	MAMP	Colorimetry	$7.5 \times 10^5$ ng/mL	5 min	[12]
G-quadruplex-hemin DNAzyme molecular beacon	MAMP	Colorimetry	0.0746 ng/mL	10 min	[58]
Aptamer-GO-CTAB-AuNP- hemin hybrid nanozyme	AMP	Colorimetry	34.1 ng/mL	1 min	<b>This work</b>
	MAMP	Colorimetry	28.6 ng/mL	1 min	<b>This work</b>

reasonable to conclude that the presumptive testing of AMP and MAMP can be selectively differentiated from other tested interferents by the rapid deep blue colour reaction transduced by the aptamer-based GO-CTAB-AuNPs peroxidase mimic biosensor.

### 3.9. Detection in mixed samples

The efficacy of the aptamer-based GO-CTAB-AuNP-hemin peroxidase mimic biosensor to detect the targeted ATS in mixed drug samples was investigated. Known adulterants such as acetaminophen, caffeine and ketamine were mixed with different concentration of MAMP and the analytical performance of the aptamer-based nano hybrid peroxidase mimic biosensor was examined. Table 3 shows the recovery efficiency of the aptamer-based nano hybrid peroxidase mimic biosensor for the detection of 100, 60 and 20  $\mu$ M MAMP in a mixed sample solution containing a fixed concentration of added adulterant (100  $\mu$ M). From the data, the recovery efficiency was at most 79.3% for 100  $\mu$ M of added MAMP in acetaminophen, 78.8% for 20  $\mu$ M of added MAMP in caffeine and 79.6% for 60  $\mu$ M of added MAMP in ketamine. In general,

we found out that the aptamer-based GO-CTAB-AuNP-hemin peroxidase mimic biosensor could detect MAMP in mixed drug samples with varying efficiency.

## 4. Conclusions

Negatively charged GO was electrostatically bonded to positively charged CTAB-AuNPs and the formed GO-CTAB-AuNP hybrid nanozyme was employed in an aptamer-based peroxidase mimic biosensor assay for the enhanced catalytic colorimetric detection of AMP and MAMP. Hemin, an iron-containing porphyrin complex was incorporated into the biosensor system and used as a catalytic signal amplifier. The structural and optical properties of GO, CTAB-AuNPs and the GO-CTAB-AuNP hybrid nanozyme were characterized using electron-based and optical techniques. Under the optimum reaction conditions, AMP and MAMP were quantitatively detected with high sensitivity and the selectivity of the biosensor was confirmed by the deep blue colour reaction specific to AMP and MAMP recognition.

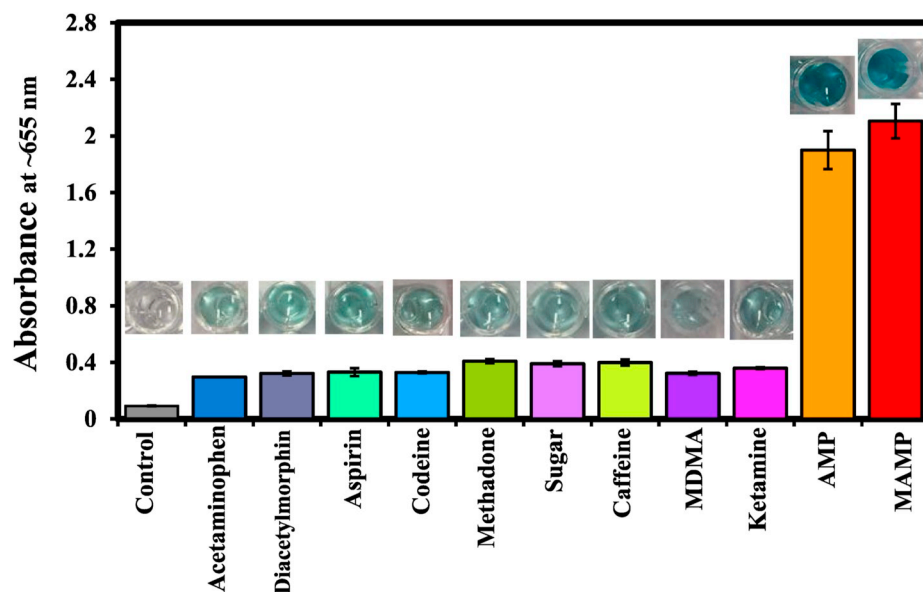


Fig. 7. Catalytic and corresponding colorimetric response of the aptamer-GO-AuNP-hemin hybrid nanozyme to AMP and MAMP in comparison to other tested drugs and substances. Concentration of ATS and other non-targets = 100  $\mu$ M; GO-CTAB-AuNP hybrid nanozyme (0.03 nM); 100  $\mu$ M DNA aptamer; 100  $\mu$ M hemin; 3000  $\mu$ M TMB; 1.2 M  $H_2O_2$ . Data recorded at  $\sim$ 1 min.

Table 3

Analytical performance of the aptamer-GO-CTAB-AuNP-hemin hybrid nanozyme peroxidase-like catalytic biosensor for MAMP detection in mixed drug samples. All data recorded at  $\sim$ 1 min.

Mixed drug (100 $\mu$ M)	MAMP added ( $\mu$ M)	Found ( $\mu$ M)	Recovery (%) $\pm$ SD (%)	RSD (%)
Acetaminophen	100	79.3	79.3 $\pm$ 4.7	4.7
	60	36.5	60.8 $\pm$ 1.8	3.0
	20	13.7	68.6 $\pm$ 0.9	1.7
Caffeine	100	70.9	70.9 $\pm$ 5.7	6.4
	60	37.8	63.1 $\pm$ 0.4	0.6
	20	15.8	78.8 $\pm$ 1.4	2.3
Ketamine	100	71.2	71.2 $\pm$ 1.9	2.0
	60	47.8	79.6 $\pm$ 0.9	1.2
	20	15.5	77.6 $\pm$ 0.3	0.4

SD = Standard deviation of three replicate measurements.

#### CRedit authorship contribution statement

**Oluwasesan Adegoke:** Conceptualization, Investigation, Methodology, Writing - original draft, Writing - review & editing. **Svetlana Zolotovskaya:** Formal analysis, Writing - review & editing. **Amin Abdolvand:** Formal analysis, Writing - review & editing. **Niamh Nic Daeid:** Conceptualization, Supervision, Writing - review & editing.

#### Declaration of competing interest

The authors declare that they have no known competing financial interests or personal relationships that could have appeared to influence the work reported in this paper.

#### Acknowledgements

Authors gratefully acknowledge the support from Leverhulme Trust for funding this work. SZ acknowledges support from EPSRC through EP/P008135/2 and EP/S017445/1.

#### Appendix A. Supplementary data

Supplementary data to this article can be found online at <https://doi.org/10.1016/j.talanta.2020.120990>.

#### References

- [1] K.M. Elkins, A.C. Weghorst, A.A. Quinn, S. Acharya, Colour quantitation for chemical spot tests for a controlled substances presumptive test database, *Drug Test. Anal.* 9 (2016) 306–310.
- [2] A. Choodum, N. Nic Daeid, Digital image-based colourimetric tests for amphetamine and methylamphetamine, *Drug Test. Anal.* 3 (2011) 277–282.
- [3] B.R. Widdop, A.C. Moffat, M.D. Osselson, B. Widdop, J. Watts (Ed.), *Clarke's Analysis of Drugs and Poisons*, Pharmaceutical Press, London, UK, 2011.
- [4] A. Argente-García, N. Jornet-Martínez, R. Harráez-Hernández, P. Campíns-Falcó, A solid colorimetric sensor for the analysis of amphetamine-like street samples, *Anal. Chim. Acta* 943 (2016) 123–130.
- [5] R.W. Freudenmann, M. Spitzer, The neuropsychopharmacology and toxicology of 3,4-methylenedioxy-N-ethyl-amphetamine (MDEA), *CNS Drug Rev.* 10 (2004) 89–116.
- [6] *World Drug Report 2015*, United Nations Division for Policy Analysis and Public Affairs, Vienna, Austria, 2015.
- [7] D. Ciccarone, Stimulant abuse: pharmacology, cocaine, methamphetamine, treatment, attempts at pharmacotherapy, *Prim. Care Clin. Off.* 38 (2011) 41–58.
- [8] S. Augenstein, Man Jailed for 4 Months until Test Showed 'meth' Was Just Epsom Salt, *Forensic Magazine*, Rockaway, NJ, 2015.
- [9] A. Harris, He Was Arrested for Meth, but the Crumbs in His Car Were Krispy Kreme Doughnut Glaze, *Miami Herald Media Company*, Miami, FL, 2016.
- [10] M. Philip, S. Fu, A review of chemical 'spot' tests: a presumptive illicit drug identification technique, *Drug Test. Anal.* 10 (2018) 95–108.
- [11] D. Favretto, F. Castagna, S. Maietti, R. Boscolo-Berto, D.S. Ferrara, When color fails: illicit blue tablets containing anabolic androgen steroids, *J. Pharmaceut. Biomed. Anal.* 83 (2013) 260–264.
- [12] S.T. Krauss, T.P. Remcho, S.M. Lipes, R. Aranda IV, H.P. Maynard III, N. Shukla, J. Li, R.E. Tontarski Jr., J.P. Landers, Objective method for presumptive field-testing of illicit drug possession using centrifugal microdevices and smartphone analysis, *Anal. Chem.* 88 (2016) 8689–8697.
- [13] R. Breslow, L.E. Overman, "Artificial enzyme" combining a metal catalytic group and a hydrophobic binding cavity, *J. Am. Chem. Soc.* 92 (1970) 1075–1077.
- [14] Z.Y. Dong, Y.G. Wang, Y.Z. Yin, J.Q. Liu, Supramolecular enzyme mimics by self-assembly, *Curr. Opin. Colloid Interface Sci.* 16 (2011) 451–458.
- [15] H. Wei, E. Wang, Nanomaterials with enzyme-like characteristics (nanozymes): next-generation artificial enzymes, *Chem. Soc. Rev.* 42 (2013) 6060–6093.
- [16] B. Garg, T. Bisht, Y.-C. Ling, Graphene-based nanomaterials as efficient peroxidase mimetic catalysts for biosensing applications: an overview, *Molecules* 20 (2015) 14155–14190.
- [17] Y. Song, K. Qu, C. Zhao, J. Ren, X. Qu, Graphene oxide: intrinsic peroxidase catalytic activity and its application to glucose detection, *Adv. Mater.* 22 (2010) 2206–2210.
- [18] N.R. Nirala, S. Abraham, V. Kumar, A. Bansal, A. Srivastava P.S. Saxena, Colorimetric detection of cholesterol based on highly efficient peroxidase mimetic activity of graphene quantum dots, *Sens. Actuators B Chem.* 218 (2015) 42–50.
- [19] L. Gao, J. Zhuang, L. Nie, J. Zhang, Y. Zhang, N. Gu, T. Wang, J. Feng, D. Yang, S. Perrett, X. Yan, Intrinsic peroxidase-like activity of ferromagnetic nanoparticles, *Nat. Nanotechnol.* 2 (2007) 577–583.
- [20] F. Manea, F.B. Houillon, L. Pasquato, P. Scrimin, Nanozymes: gold-nanoparticle-based transphosphorylation catalysts, *Angew. Chem. Int. Ed.* 43 (2004) 6165–6169.
- [21] S. Biswas, P. Tripathi, N. Kumar, S. Nara, Gold nanorods as peroxidase mimetics and its application for colorimetric biosensing of malathion, *Sens. Actuators B Chem.* 231 (2016) 584–592.

- [22] W. Shi, Q. Wang, Y. Long, Z. Cheng, S. Chen, H. Zheng, Y. Huang, Carbon nanodots as peroxidase mimetics and their applications to glucose detection, *Chem. Commun.* 47 (2011) 6695–6697.
- [23] C. Zheng, W. Ke, T. Yin, X. An, Intrinsic peroxidase-like activity and the catalytic mechanism of gold@carbon dots nanocomposite, *RSC Adv.* 6 (2016) 35280–35286.
- [24] K.S. Lee, M.A. El-Sayed, Gold and silver nanoparticles in sensing and imaging: sensitivity of plasmon response to size, shape, and metal composition, *J. Phys. Chem. B* 110 (2006) 19220–19225.
- [25] V. Georgakilas, M. Otyepka, A.B. Bourlinos, V. Chandra, N. Kim, K.C. Kemp, P. Hobza, R. Zboril, K.S. Kim, Functionalization of graphene: covalent and non-covalent approaches, derivatives and applications, *Chem. Rev.* 112 (2012) 6156–6214.
- [26] G.H. Jin, E. Ko, M.K. Kim, V.-K. Tran, S.E. Son, Y. Geng, Won Hur, G.H. Seoung, Graphene oxide-gold nanozyme for highly sensitive electrochemical detection of hydrogen peroxide, *Sens. Actuators B Chem.* 274 (2018) 201–209.
- [27] S.R. Ahmed, K. Takemeura, T.-C. Li, N. Kitamoto, T. Tanaka, T. Suzuki, E.Y. Park, X.F. Duan, Graphene-supported peroxidase-like graphene-gold nanoparticle hybrids for the visible detection of norovirus-like particles, *Biosens. Bioelectron.* 87 (2017) 558–565.
- [28] J. Simplicio, Hemin monomers in micellar sodium lauryl sulfate. Spectral and equilibrium study with cyanide, *Biochemistry* 11 (1972) 2525–2528.
- [29] T. Xue, S. Jiang, Y.Q. Qu, Q. Su, R. Cheng, S. Dubin, C.Y. Chiu, R. Kaner, Y. Huang, X.F. Duan, Graphene-supported hemin as a highly active biomimetic oxidation catalyst, *Angew. Chem. Int. Ed.* 51 (2012) 3822–3825.
- [30] T. Hermann, D.J. Patel, Adaptive recognition by nucleic acid aptamers, *Science* 287 (2000) 820–825.
- [31] M. McKeague, M.C. DeRosa, Challenges and opportunities for small molecule aptamer development, *J. Nucleic Acids* 2012 (2012) 1–20.
- [32] H. Sun, Y. Zu, A Highlight of recent advances in aptamer technology and its application, *Molecules* 20 (2015) 11959–11980.
- [33] K. Mao, Z. Yang, P. Yu, Z. Xu, Z. Wang, X. Li, G-quadruplex-hemin DNAzyme molecular beacon probe for the detection of methamphetamine, *RSC Adv.* 6 (2016) 62754–62759.
- [34] T.K. Sau, C.J. Murphy, Room temperature, high-yield synthesis of multiple shapes of gold nanoparticles in aqueous solution, *J. Am. Chem. Soc.* 126 (2004) 8648–8649.
- [35] W.S. Hummers Jr., R.E. Offeman, Preparation of graphitic oxide, *J. Am. Chem. Soc.* 80 (1958) 1339–1339.
- [36] O. Adegoke, P.B.C. Forbes, L-cysteine-capped core/shell/shell quantum dot-graphene oxide nanocomposite fluorescence probe for polycyclic aromatic hydrocarbon detection, *Talanta* 146 (2016) 780–788.
- [37] B. Liu, S. Salgado, V. Maheshwari, J. Liu, Janus DNA orthogonal adsorption of graphene oxide and metal oxide nanoparticles enabling stable sensing in serum, *Curr. Opin. Colloid Interface* 26 (2016) 41–49.
- [38] A. Lerf, H. He, M. Forster, J. Klinowski, Structure of graphite oxide revisited, *J. Phys. Chem. B* 102 (1998) 4477–4482.
- [39] E. Priyadarshini, N. Pradhan, Gold nanoparticles as efficient sensors in colorimetric detection of toxic metal ions: a review, *Sens. Actuators B Chem.* 238 (2017) 888–902.
- [40] K. Jain, K.S. Lee, I.H. El-Sayed, M.A. El-Sayed, Calculated absorption and scattering properties of gold nanoparticles of different size, shape, and composition: applications in biological imaging and biomedicine, *J. Phys. Chem. B* 110 (2006) 7238–7248.
- [41] E. Oliveira, C. Núñez, H.M. Santos, J. Fernández-Lodeiro, A. Fernández-Lodeiro, J.L.C. Capelo, Lodeiro, Revisiting the use of gold and silver functionalised nanoparticles as colorimetric and fluorometric chemosensors for metal ions, *Sens. Actuators B Chem.* 212 (2015) 297–328.
- [42] D. Li, M.B. Muller, S. Gilje, R.B. Kaner, G.G. Eallace, Processable aqueous dispersions of graphene nanosheets, *Nat. Nanotechnol.* 3 (2008) 101–105.
- [43] S. Saxena, T.A. Tyson, S. Shukla, E. Negusse, H. Chen, J. Bai, Investigation of structural and electronic properties of graphene oxide, *Appl. Phys. Lett.* 99 (2011) 013104.
- [44] V.R. Patel, Y.K. Agrawal, Nanosuspension: an approach to enhance solubility of drugs, *J. Adv. Pharm. Technol. Res.* 2 (2011) 81–87.
- [45] Z. Çiplak, N. Yildiz, A. Çalimli, Investigation of graphene/Ag nanocomposites synthesis parameters for two different synthesis methods, *Fullerenes, Nanotub. Carbon Nanostruct.* 23 (2014) 361–370.
- [46] P. Weerathunge, R. Ramanathan, R. Shukla, T.K. Sharma, V. Bansal, Aptamer-controlled reversible inhibition of gold nanozyme activity for pesticide sensing, *Anal. Chem.* 86 (2014) 11937–11941.
- [47] T.K. Sharma, R. Ramanathan, P. Weerathunge, M. Mohammadtaheri, H.K. Daima, R. Shukla, V. Bansal, Aptamer-mediated 'turn-off/turn-on' nanozyme activity of gold nanoparticles for kanamycin detection, *Chem. Commun.* 50 (2014) 15856–15859.
- [48] R. Das, A. Dhiman, A. Kapil, V. Bansal, T.K. Sharma, Aptamer-mediated colorimetric and electrochemical detection of *Pseudomonas aeruginosa* utilizing peroxidase-mimic activity of gold NanoZyme, *Anal. Bioanal. Chem.* 411 (2019) 1229–1238.
- [49] R. Das, B. Chatterjee, A. Kapil, T.K. Sharma, Aptamer-NanoZyme mediated sensing platform for the rapid detection of *Escherichia coli* in fruit juice, *Sens. Biosens. Res.* 27 (2020) 100313.
- [50] N. Varghese, U. Mogera, A. Govindaraj, A. Das, P.K. Maiti, A.K. Sood, C.N. Rao, Binding of DNA nucleobases and nucleosides with graphene, *ChemPhysChem* 10 (2009) 206–210.
- [51] H. Bisswanger, Enzyme assays, *Perspect. Sci* 1 (2014) 41–55.
- [52] H. Lineweaver, D. Burk, The determination of enzyme dissociation constants, *J. Am. Chem. Soc.* 56 (1934) 658–666.
- [53] M. Li, J. Yang, Y. Ou, Y. Shi, Li Liu, C. Sun, H. Zheng, Y. Long, Peroxidase-like activity of 2',7'-difluorofluorescein and its application for galactose detection, *Talanta* 182 (2018) 422–427.
- [54] "Color test reagents/kits for preliminary identification of drugs of abuse" (PDF), Law Enforcement and Corrections Standards and Testing Program, July 2000.
- [55] Claire Cole, L. Jones, J. McVeigh, A. Kicman, Q. Syed, M.A. Bellis, "CUT: A Guide to Adulterants, Bulking Agents and Other Contaminants Found in Illicit Drug" (PDF), (April 2000).
- [56] K. Mao, Z. Yang, J. Li, X. Zhuo, X. Li, J. Hu, A novel colorimetric biosensor based on non-aggregated Au@Ag core-shell nanoparticles for methamphetamine and cocaine detection, *Talanta* 175 (2017) 338–346.
- [57] A. Choodum, P. Kanatharana, W. Wongniramaikul, N. NicDaeid, A sol-gel colorimetric sensor for methamphetamine detection, *Sens. Actuators B Chem.* 215 (2015) 553–560.
- [58] K. Mao, Z. Yang, P. Du, Z. Xu, Z. Wang, X. Li, G-quadruplex-hemin DNAzyme molecular beacon probe for the detection of methamphetamine, *RSC Adv.* 6 (2016) 62754–62759.